Autocatalysis and Selective Oxidative Etching Induced Synthesis of Platinum−Copper Bimetallic Alloy Nanodendrites Electrocatalysts

Mingxing Gong,[‡,§] Gengtao Fu,[‡,§] Yu Chen,*[,†] Yawen Tang,*[,‡] and Tianhong Lu[‡]

[†]School of Materials Science and Engineering, Shaanxi Normal University, Xi'an 710062, China

[‡]Jiangsu Key Laboratory of New Power Batteries, School of Chemistry and Materials Science, Nanjing Normal University, Nanjing 210023, China

S *Supporting Information*

ABSTRACT: The controllable synthesis of noble metal alloy nanostructures with highly branched morphology has attracted much attention because of their specific physical and chemical properties. This article reports the synthesis of platinum−copper bimetallic alloy nanodendrites (Pt−Cu BANDs) by a facile, one-pot, templateless, and seedless hydrothermal method in the presence of poly(allylamine hydrochloride) (PAH) and formaldehyde (HCHO). The morphology, composition, and structure of Pt−Cu BANDs are fully characterized by various physical techniques, demonstrating Pt−Cu BANDs are highly alloying, porous, and self-supported nanostructures. The formation/growth mechanism of Pt−Cu BANDs is explored and discussed based on the experimental observations. The autocatalytic growth and interdiffusion are responsible for the formation of Pt−Cu alloy whereas selective oxidative etching results in dendritic morphology of Pt−Cu alloy nanostructures. In addition, the electrocatalytic activity and stability of Pt−Cu BANDs for the methanol oxidation reaction (MOR) are investigated by various electrochemical techniques. The synthesized Pt−Cu BANDs show higher electrocatalytic activity and stability than commercially available Pt black.

KEYWORDS: *platinum−copper alloy, nanodendrites, polyallylamine, electrocatalytic activity, methanol oxidation reaction*
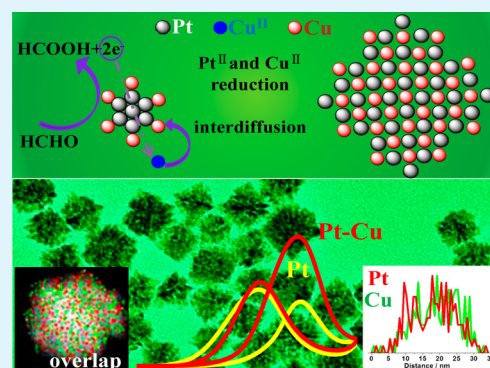
1. INTRODUCTION

Noble-metal Pt nanocrystals with various sizes, dimensions, and morphologies are technologically important nanomaterials because of their unique physical and chemical properties that different from their bulk state counterparts. It has been demonstrated that the intrinsic properties of Pt nanocrystals can be dramatically enhanced by shape and structural variation. For example, the highly branched Pt nanodendrites exhibit superior catalytic/electrocatalytic activity and stability for many important reactions because of their attractive structural features such as porosity, high surface area, interconnected nanostructure, excellent electrical connectivity, and high density of twinned defects.[1−12]

Due to high cost and rare reserve, it is highly desirable to minimize the usage amount of Pt metal. Introducing a second metal to form Pt-based bimetallic alloy, intermetallic nanocrystals, and cell−shell nanostructures has proven to be an effective strategy to reduce the cost of Pt and simultaneously improve the catalytic/electrocatalytic activity because of the modified geometric and electronic structures of Pt nanocrystals.[13−35] Recently, Pt-based bimetallic nanodendrites, such as Pt−Ni,[15,16] Pt−Pd,[17−21] Pt−Co,[22] Pt−Au,[23,24] and Pt−Cu[25,36] nanodendrites have been synthesized using various methods, including cochemical reduction,[18,20,25] thermal decomposition,[15,16] seed growth,[15,17,19,21,23] hard-templating synthesis,[22] and galvanic replacement,[24] etc. For instance, Pt−Ni nanodendrites were synthesized by reducing expensive platinum(II) acetylacetonate [Pt(acac)$_2$] and nickel(II) acetylacetonate [Ni(acac)$_2$] in complex octadecene (ODE), oleylamine (OAm), didodecyldimethylammonium bromide (DDAB) organic system at very high temperature (200 °C).[15] Highly interesting Pt−Pd bimetallic nanodendrites were prepared by reducing potassium tetrachloroplatinate(II) (K$_2$PtCl$_4$) with L-ascorbic acid (AA) in the presence of 9 nm truncated octahedral Pd seeds, with the addition of poly(vinylpyrrolidone) (PVP) as a stabilizer.[19] Despite those impressive advances in synthesis, many established methods suffer from relatively high cost, high reaction temperature, and complex reaction step.

Among various Pt-based bimetallic nanostructures, Pt−Cu bimetallic nanostructures with well-defined morphologies have attracted considerable attention due to their numerous applications in industrial catalysis and fuel cells.[3,25,36−48] For example, PtCu$_3$ nanocages were prepared by using chloroplatinic acid hexahydrate (H$_2$PtCl$_6$·6H$_2$O), copper(II) acetylacetonate [Cu(acac)$_2$] as precursors, and cetyltrimethylammonium

bromide (CTAB), OAm as stabilizers under one-pot hydrothermal condition (170 °C).[47] Pt−Cu nanocubes were also prepared by simultaneous reduction of platinum(II) acetylacetonate $[Pd(acac)_2]$ and $Cu(acac)_2$ by 1,2-tetradecanediol (TDD) in ODE as solvent, which also contained OAm, tetraoctylammonium bromide (TOAB), and a trace amount of 1-dodecanethiol (DDT).[48] More recently, dendritic-like Pt−Cu nanostructure were synthesized through a two step coreduction method.[36] These Pt−Cu bimetallic nanostructures (i.e., nanocages, nanocubes, nanodendrites) exhibited the enhanced electrocatalytic activity for MOR, due to their unique structure and the bifunctionality of Pt and Cu. However, up to now, a facile one-pot synthesis of Pt−Cu alloy nanodendrites are still rarely reported.[25,36] So undoubtedly, developing a convenient and environmentally benign method to synthesize highly branched Pt−Cu alloy nanostructures is of high significance owing to fascinating physical and chemical properties of nanodendrites. As an advantage over organic systems, based on autocatalytic growth and selective oxidative etching mechanisms, we here describe the facile synthesis of Pt−Cu bimetallic alloy nanodendrites (Pt−Cu BANDs) using a facile one-step aqueous-phase coreduction method. The as-prepared Pt−Cu BANDs exhibit remarkably improved electrocatalytic activity and stability for MOR over commercially available Pt black.

2. EXPERIMENTAL SECTION

2.1. Reagents and Chemicals. Poly(allylamine hydrochloride) (PAH, weight-average molecular weight, M_w = 150 000) was supplied from Nitto Boseki Co., Ltd. (Tokyo, Japan). Potassium tetrachloroplatinate(II) (K_2PtCl_4), cupric chloride ($CuCl_2$), methanol (CH_3OH), and formaldehyde (HCHO) solution (40%) were purchased from Sinopharm Chemical Reagent Co., Ltd. (Shanghai, China). Commercial Pt black was purchased from Johnson Matthey Corporation. Other reagents were of analytical reagent grade and used without further purification. All the aqueous solutions were prepared with Millipore water having a resistivity of 18.2 MΩ.

2.2. Preparation of Pt−Cu BANDs. In a typical synthesis, 1.0 mL of 50 mM K_2PtCl_4, 1.0 mL of 50 mM $CuCl_2$, and 2.3 mL of 0.43 M PAH (molarity of PAH given with respect to the repeating unit) aqueous solutions were added to 5.0 mL water with continued stirring. After adjusting solution pH to 3.0, 2.0 mL of HCHO solution (40%) was added into the mixture solution and mechanically stirred for 10 min. Then, the resultant mixture was transferred to a 25.0 mL Teflon-lined stainless-steel autoclave and was then heated at 140 °C for 4 h under hydrothermal conditions. After being cooled to room temperature, Pt−Cu BANDs were obtained by centrifugation at 19 000 rpm for 10 min, and further washed with acetic acid for 12 h to remove redundant PAH.[49,50]

2.3. Electrochemical Instrument. All electrochemical experiments were carried out on a CHI 660D electrochemical workstation. A standard three-electrode system was used for all electrochemical experiments, which consisted of a platinum wire as the auxiliary electrode, a saturated calomel reference electrode (SCE) protected by Luggin capillary with KCl solution as the reference electrode, and a catalyst modified glassy carbon electrode as the working electrode. All potentials in this study were reported with respect to the SCE. All electrochemical measurements were carried out at 30 ± 1 °C.

An evenly distributed suspension of catalyst was prepared by ultrasonic the mixture of 10 mg catalyst and 5 mL H_2O for 30 min, and 8 μL of the resulting suspension was drop-cast onto the surface of the glassy carbon electrode. After drying at room temperature, 3 μL of Nafion solution (5 wt %) was covered on the modified electrode surface and allowed drying again. Thus, the working electrode was obtained, and the specific loading of metal on the electrode surface was about 226 μg cm^{-2}. Electrochemical measurements were conducted in

N_2-saturated 0.5 M H_2SO_4 solution or N_2-saturated 0.5 M H_2SO_4 solution with 1.0 M CH_3OH.

2.4. Instruments. Transmission electron microscopy (TEM) images were made on a JEOL JEM-2100F transmission electron microscopy operated at an accelerating voltage of 200 kV. The samples were prepared by placing a drop of the colloidal solution or catalyst powder dispersion in ethanol solution (99%) on a carbon film coated Ni grid (3 mm, 300 mesh), followed by drying under ambient conditions. Energy dispersive X-ray (EDX) analysis was carried out on a JEOL JSM-7600F scanning electron microscopy. X-ray diffraction (XRD) patterns were obtained with a Model D/max-rC X-ray diffractometer using Cu Kα radiation source (λ = 1.5406 Å) and operating at 40 kV and 100 mA. X-ray photoelectron spectroscopy (XPS) measurements were carried out on a Thermo VG Scientific ESCALAB 250 spectrometer with an Al Kα radiator, and the vacuum in the analysis chamber was maintained at about 10^{-9} mbar. The binding energy was calibrated by means of the C 1s peak energy of 284.6 eV.

3. RESULTS AND DISCUSSION

3.1. Physicochemical Characterization of Pt−Cu BANDs. Poly(allylamine hydrochloride) (PAH), a positively charged polyelectrolyte with a large number of primary amine groups, has excellent coordination capability, good hydrophilic property and high chemical stability. Our previous works have demonstrated that PAH can efficiently serve as complex-forming agent, capping agent, and facet-selective agent to control the synthesis of Pt or Pd nanostructures with well-defined morphologies.[51−53] Pt−Cu bimetallic alloy nanodendrites (Pt−Cu BANDs) were readily achieved by reducing K_2PtCl_4 and $CuCl_2$ precursors with HCHO in aqueous PAH solution at 140 °C for 4 h.

The low resolution TEM image reveals the obtained products are well-dispersed and complete dendritic-like structure with an average particle diameter of 35 nm (Figure 1A and right-top insert), demonstrating the high-yield formation of nanodendrites (~100%). The selected-area
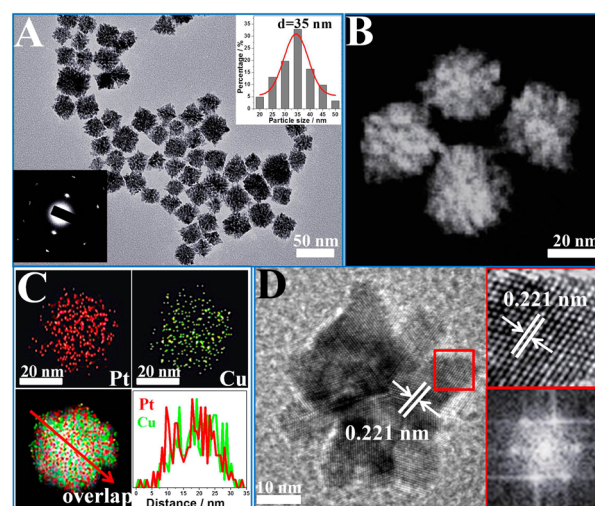

Figure 1. (A) Low resolution TEM image of Pt−Cu BANDs. The right-top inset shows the corresponding size distribution histogram; the left-bottom inset shows the corresponding SAED pattern. (B) HAADF-STEM image of Pt−Cu BANDs. (C) EDX elemental mapping patterns and EDX line scanning profiles of Pt−Cu BANDs. (D) HRTEM image of Pt−Cu BANDs. The right-top inset shows magnified HRTEM images recorded from regions marked by squares in panel D; the right-bottom inset shows the FFT pattern of a crystalline grain.

electron diffraction (SAED) image of an individual nano-dendrite demonstrates that products are crystalline structure (left-bottom insert in Figure 1A). The dendritic structure of products was clearly visualized by a high-angle annular dark-field scanning TEM (HAADF-STEM) image. Each Pt−Cu nanodendrite is actually a three dimensionally interconnected porous nanostructure, which is consisted of smaller crystallites with diameters of about 3−6 nm (Figure 1B). EDX spectrum elemental mapping patterns and EDX line scanning profile show a homogeneous distribution of both Pt and Cu in the dendritic shape (Figure 1C), which is indicative of Pt−Cu alloy formation.[20] The Pt/Cu atomic ratio determined by EDX analysis is 52:48, in good agreement with the Pt/Cu atomic ratio in the initial reaction system (50:50). High resolution TEM (HRTEM) image further shows that each Pt−Cu nanodendrite is composed of many crystalline grains with their crystallographic orientations (Figure 1D). The interplanar spacing with 0.221 nm is observed on Pt−Cu BANDs surface (right-top insert in Figure 1D), which is smaller than the {111} lattice spacing (0.226 nm) of face-centered cubic (*fcc*) Pt crystal. This not only confirms that Pt−Cu BANDs are perfectly {111} facets but also indirectly verifies the formation of Pt−Cu alloy. The corresponding fast Fourier transform (FFT) pattern shows the 6-fold rotational symmetry of the diffraction spots (right-bottom insert in Figure 1D), fuerther confirming that Pt−Cu BANDs are actually presented by {111} facets.

The crystal structure of Pt−Cu BANDs was investigated by XRD pattern, demonstrating that Pt−Cu BANDs could be identified as *fcc* structure (Figure 2). The diffraction peaks of
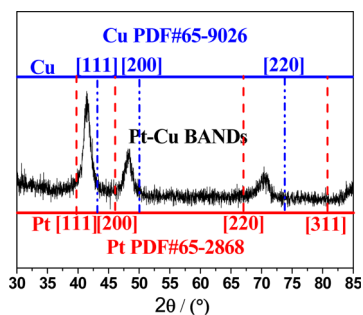

Figure 2. XRD pattern of Pt−Cu BANDs.

products are located between those of pure *fcc* Pt (PDF#04-0802) and Cu (PDF#04-0836) crystal phases, and no characteristic peaks of Cu or its oxides are detected, which is indicative of Pt−Cu alloy formation.[37] The lattice parameter value (a) of Pt−Cu BANDs is calculated to be 0.3778 nm, smaller than that of bulk Pt (PDF#04-0802 Pt, a = 0.3922 nm), reflecting the lattice contraction because of the partial substitution of Pt by Cu. Based on Vegard's law, the alloying Cu content in Pt−Cu BANDs (with respect to Pt) is estimated to be 46.8 atomic% from observed unit cell parameters according to $a = a_0 - kx_{Cu}$.[46] Where a is the measured lattice parameter of Pt−Cu alloy, a_0 is the lattice parameter of pure Pt (3.922 Å), k is a constant (0.308 Å), and x_{Cu} is the molar ratio of Cu in the bimetallic alloy. Clearly, the atomic fraction of Cu in the alloy of Pt−Cu BANDs (x_{Cu} = 46.8 at. %) is very close to the EDX compositions of Pt−Cu BANDs (atomic ratio of Pt and Cu is 52:48), indicating almost all Cu atoms entered into Pt lattice to form Pt−Cu alloy, and consequently Pt−Cu BANDs have very high alloying degree. According to Scherrer

equation, the average particle size (d_{XRD}) of the small Pt−Cu grains in Pt−Cu BANDs is calculated to be 4.8 nm, in consistent with TEM observation.

The surface composition of Pt−Cu BANDs was analyzed by XPS. The Pt 4f spectrum show the percentage of Pt^0 species is 88.4% (Figure 3A). The Cu 2p spectrum exhibits peaks at 932.4
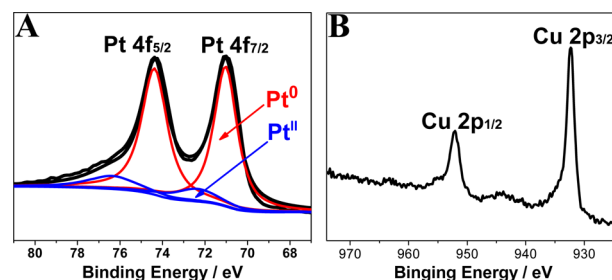

Figure 3. XPS spectra of Pt−Cu BANDs in (A) Pt 4f and (B) Cu 2p regions.

(Cu 2p3/2) and 952.4 eV (Cu 2p1/2), indicative of elemental Cu^0 (Figure 3B). Thus, XPS measurements demonstrate that Pt^{II} and Cu^{II} precursors are reduced successfully. Based on the integrated area and sensitivity factors of Pt 4f and Cu 2p, the surface atomic ratio of Pt and Cu atoms is calculated to be 48:52, in consistent with bulk composition obtained from EDX analysis, which is also indicative of Pt−Cu alloy formation.[27] Meanwhile, Pt 4f binding energy in Pt−Cu BANDs negatively shift ca. 0.41 eV compared to that in commercial Pt black (Supporting Information (SI) Figure S1). The negative shifts of the Pt 4f binding energy show the evident change in the Pt electronic structure, further confirming the formation of Pt−Cu alloy. The change of Pt electronic structure mainly originates from electron donation from the Cu to Pt because of different electronegativity.[44]

It is known that the standard reduction potential for Cu^{2+}/Cu (0.340 V vs RHE) is much lower than that of $PtCl_4^{2-}$/Pt (0.755 V vs RHE) pairs, and usually the ones with high standard reduction potential can be reduced preferentially.[29] According to thermodynamical view, a Pt-rich core and a Cu-rich shell type Pt−Cu bimetallic nanostructures should be predominant products in the wet-chemical synthetic process because of their different standard reduction potential.[28] Surprisingly, the high alloying Pt−Cu BANDs are achieved in the present synthesis. Indeed, the single-component Cu^{II} precursor cannot be reduced even within a longer reaction time (140 °C, 48 h), indicating that the reduction of Cu^{II} precursor is facilitated by the preformed Pt crystal nuclei through the autocatalytic growth mechanism.[28,29] The deposited surface Cu atoms are then mixed with Pt atoms through an interdiffusion process because of thermal energy,[28,30] accompanying the simultaneously direct reduction of Pt^{II} precursor, and Pt−Cu alloy ultimately forms (Scheme 1).

At present, noble metal nanodendrites were obtained mainly by aggregation-based nanocrystal rapid-growth (fast reaction), kinetically controlled heterogeneous seeded growth (slow reaction), and oxidative etching (slow reaction).[10,11] In our synthesis, the reduction rate of Pt^{II} and Cu^{II} precursors is very slow (4 h). Thus, the aggregation-based nanocrystal rapid-growth mechanism is ruled out. Moreover, heterogeneous seeded growth mechanism is also ruled out because no seeds are used in synthesis. To better understand the formation/

Scheme 1. Formation Mechanism of Pt−Cu Alloy
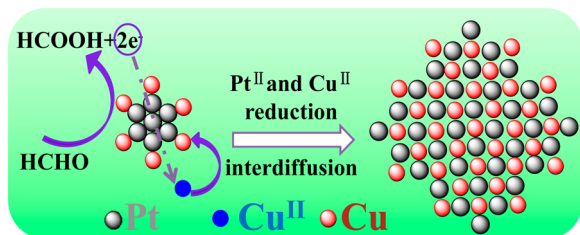
growth mechanism of Pt−Cu BANDs, growth intermediates of Pt−Cu BANDs were collected at different reaction times and characterized by TEM. At 2 h, very little precipitate was obtained by centrifugation. TEM image shows Pt−Cu nanodendrites with branched structure (average size ~15 nm) have already formed at 2 h (Figure 4A). With increasing reaction
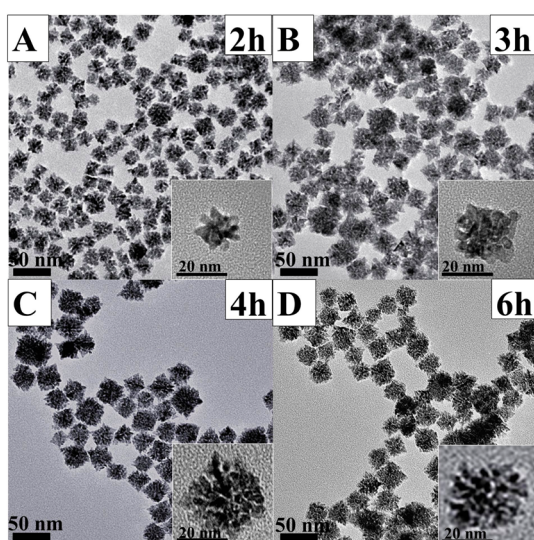

Figure 4. TEM images of Pt−Cu nanodendrites samples collected at different growth stages: (A) 2, (B) 3, (C) 4, and (D) 6 h.

times, the diameters of Pt−Cu nanodendrites expand to ~25 and ~35 nm at 3 and 4 h, respectively (Figure 4B and C). When the reaction time is further extended to 6 h, no significant change is observed for Pt−Cu BANDs in terms of both size and shape (Figure 4D). The chemical compositions of intermediates at the different growth stages were also estimated by EDX analyses. The Pt/Cu atomic ratio of all Pt−Cu intermediates is close to 1:1 (SI Figure S2), demonstrating that the Pt−Cu alloy nanoparticles have already formed at 2 h. The facts further confirm the formation of Pt−Cu alloy originates from the autocatalytic growth mechanism, as shown in Scheme 1.

In whole reaction process, no single small nanoparticles are observed in a series of TEM images. Moreover, the size distributions of Pt−Cu nanodendrites are narrow. In a controlled experiment without Cu^{2+} ion, monodisperse Pt nanocubes with six {100} facets were obtained (SI Figure S3), in consistent with our previous report.[51] Based on the above experimental observations, we can infer that the introduction of Cu^{2+} ion into the reaction system is critical to the dendritic morphology of Pt−Cu BANDs. After heating Pt nanocubes in air-saturated $CuCl_2$ solution at 140 °C for 48 h, cubic shape of Pt nanocubes still preserves (SI Figure S4), demonstrating that

oxidative etching cannot occur on Pt nanocubes under present experimental conditions. In another controlled experiment, the irregular Pt−Cu multipods are obtained by displacing the air with N_2 to eliminate typical etchant O_2 (SI Figure S5). These facts indicate the introduction of Cu^{2+} ion source facilitates the anisotropic growth of Pt nanostructures because of the change in seed surface energy, similar to Cu^{2+}-assisted synthesis of various Pd nanostructures,[54−56] including Pd tripods,[54] Pd nanorods,[55] and hexoctahedral Au−Pd alloy nanocrystals.[56] Compared with the synthetic parameters of irregular Pt−Cu multipods (i.e., no O_2), it is safe to state that selective oxidative etching on Cu atoms is critical in determining the morphology of Pt−Cu BANDs. Since Pt is an effective catalyst for oxygen reduction reaction, the dissolved O_2 can be reduced on the Pt surface, where the electrons required for this reduction come from the dissolution of Cu.[29] Consequently, some of Cu atoms on the Pt crystal facets can be selectively oxidized back to Cu^{2+} species by O_2 and dissolve into the solution (Scheme 2). In this

Scheme 2. Progressive Formation of Pt−Cu BANDs
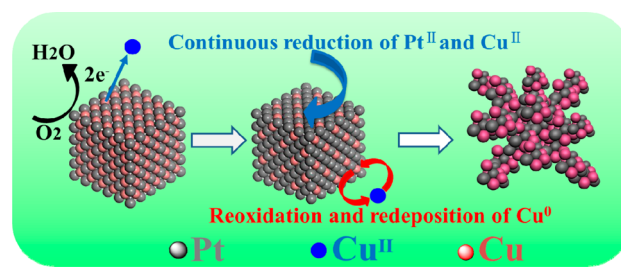
case, the ordered surface structure of Pt crystal facets is partially destroyed, resulting in the coexistence of discontinuous Cu and Pt adatoms region on the formed Pt seed surface. Subsequently, the continuous anisotropic growth of crystal nuclei (the continuous addition of Pt and Cu atoms reduced by HCHO on different adatoms layers) as well as periodic deposition and reoxidation of Cu atoms on the growing nanoparticles ultimately result in the formation of extensively branched morphology (Scheme 2).

3.2. Electrocatalytic Tests. The electrochemical properties of Pt−Cu BANDs were first investigated by cyclic voltammetry (CV) in a 0.5 M H_2SO_4 solution (Figure 5). By using hydrogen adsorption−desorption method in conjunction with CV, the electrochemically surface areas (ECSA) is determined to be 23.5 $m^2\ g^{-1}$ for Pt−Cu BANDs, 35.8% larger than that of the commercial Pt black (17.3 $m^2\ g^{-1}$), which is ascribed to inherent porous structure of Pt−Cu BANDs and small particle size of Pt−Cu grains in Pt−Cu BANDs ($d_{xrd-Pt-Cu\ BANDs}$ = 4.8 nm vs $d_{xrd-Pt\ black}$ = 8.5 nm). This result clearly reveals that Pt−Cu BANDs are electrochemically more accessible, which is very important for the electrocatalytic reactions.[17,37]

Highly branched Pt-base bimetallic alloy nanodendrites with low precious metal loading, high surface area, and high density of twinned defects should be very desirable for electrocatalysis. Herein, methanol was selected as a model molecule for studying the electrocatalytic activity of Pt−Cu BANDs because of its important application in direct methanol fuel cells (DMFCs). The mass activity of electrocatalysts (i.e., the currents are normalized to the metal mass) is generally taken as an index to assess the applicability of electrocatalysts. The electrocatalytic properties of Pt−Cu BANDs and commercial Pt black for methanol oxidation reaction (MOR) were first
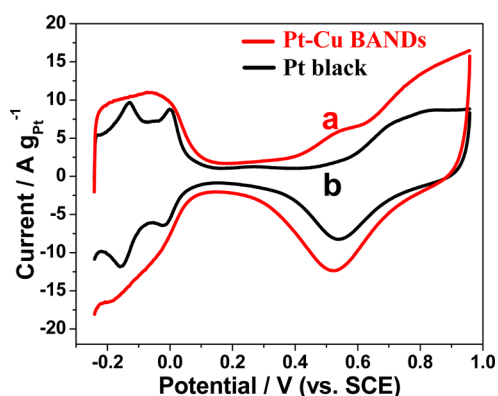
7304

dx.doi.org/10.1021/am500656j | ACS Appl. Mater. Interfaces 2014, 6, 7301−7308

Figure 5. CV curves for (a) Pt−Cu BANDs and (b) commercial Pt black in N_2-saturated 0.5 M H_2SO_4 solution at a scan rate of 50 mV s^{-1}. The ECSA of Pt electrocatalyst was calculated by measuring the charge collected in the hydrogen adsorption/desorption region after double-layer correction and assuming a value of 210 μC cm^{-2} for the adsorption of a hydrogen monolayer.[37]

investigated by CV, using the same Pt loading (Figure 6A). Two obvious anodic peaks (i.e., methanol oxidation peak at
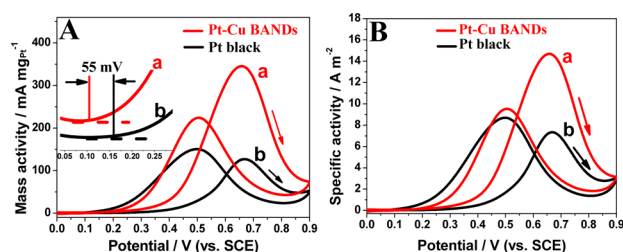

Figure 6. CV curves for (a) Pt−Cu BANDs and (b) commercial Pt black in N_2-saturated 0.5 M H_2SO_4 + 1.0 M CH_3OH solution at a scan rate of 50 mV s^{-1}, which are normalized to (A) Pt mass (mass activity) and (B) the real Pt ECSA (specific activity), respectively. Arrows indicate the potential scan direction.

higher potential and intermediate carbonaceous species oxidation peak at lower potential), which are typical features of methanol electrooxidation reaction, are observed on both Pt−Cu BANDs and Pt black during the positive and negative scan directions. Compared to Pt black, the onset oxidation potential and oxidation peak potential of methanol on Pt−Cu BANDs negatively shift ca. 55 and 15 mV, respectively, which result in a large enhancement in electrocatalytic activity at low potential.[27] For example, the methanol oxidation current at 0.5 V (a typical working potential for direct methanol fuel cells) are 40.3 and 11.3 mA mg^{-1} on Pt−Cu BANDs and Pt black, respectively. Obviously, the electrocatalytic activity of Pt−Cu BANDs has been enhanced remarkably at this potential compared to Pt black. It is worthwhile noting that methanol oxidation peak potential on Pt−Cu BANDs is also lower than that on various Pt−Cu bimetallic nanostructures reported previously,[25,38,39,42,44] further indicating Pt−Cu BANDs hold promise as potentially practical electrocatalysts for the MOR.

Besides the mass activity for evaluating the effectiveness of Pt utilization, the specific activity (i.e., the current is normalized to ECSA of electrocatalysts) is often used to evaluate the actual value of the intrinsic activity of electrocatalysts. Thus, the electrocatalytic properties of Pt−Cu BANDs and commercial Pt black for the MOR were further studied by CV, using the same ECSA value (Figure 6B). As observed, specific current

density of methanol oxidation on Pt−Cu BANDs (5.61 A m_{Pt}^{-2}) is 3.5 times higher than that on Pt black (1.62 A m_{Pt}^{-2}) at 0.5 V, confirming that Pt−Cu BANDs have better electrocatalytic activity than Pt black. Meanwhile, methanol oxidation peak current on Pt−Cu BANDs (15.1 A m_{Pt}^{-2}) is also higher than those of Pt nanowires (8.4 A m_{Pt}^{-2}), Pt−Cu nanocrystals (12.6 A m_{Pt}^{-2}), Pt−Ni nanocrystals (13.4 A m_{Pt}^{-2}), Pt−Co nanocrystals (10.7 A m_{Pt}^{-2}), and Pt−Fe nanocrystals (12 A m_{Pt}^{-2}),[44] which further indicates that Pt−Cu BANDs show competitive electrocatalytic activity for the MOR. In the Pt−Cu alloy system, Cu can donate electron density to the incompletely filled d-bands of Pt (i.e., electronic effect) thereby changing the adsorption energies of reactants and reaction products. Moreover, Cu can also decrease the average number of contiguous Pt atoms at the surface that participate in the reaction by simple dilution (i.e., geometric effect) thereby changing the adsorption orientation and/or strength of reactants and reaction products.[57] Thus, alloying Pt with Cu should be a key factor for improved electrocatalytic activity of Pt−Cu BANDs for the MOR. During the MOR, Pt electrocatalysts easily lose a large amount of activity owing to the CO-like carbonaceous adsorption species (CO_{ads}) and/or unidentified non-CO_{ads} organic species. The ratio of the forward oxidation current peak (I_f) to the reverse current peak (I_b), I_f/I_b, is an important index of the poison tolerance of electrocatalysts during the MOR.[4,17] A higher ratio indicates more effective removal of the poisoning species on the electrocatalyst surface. The I_f/I_b ratio (1.5) of Pt−Cu BANDs is much higher than that (0.8) of commercially available Pt black, showing relatively better poison tolerance of Pt−Cu BANDs.

Superior poison tolerance of Pt−Cu BANDs was confirmed by CO_{ads}−stripping tests (Figure 7A). The onset potential and
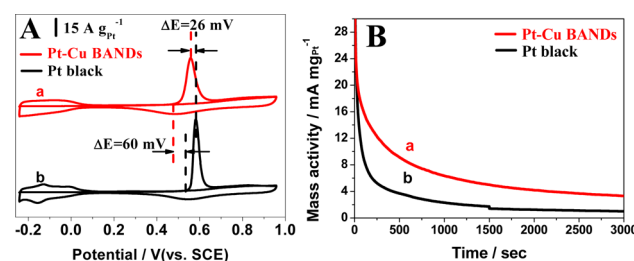

Figure 7. (A) CV curves for preadsorbed CO at (a) Pt−Cu BANDs and (b) commercial Pt black in N_2-saturated 0.5 M H_2SO_4 solution at the scan rate of 50 mV s^{-1}. (B) Chronoamperometry curves for (a) Pt−Cu BANDs and (b) commercial Pt black in N_2-saturated 0.5 M H_2SO_4 + 1.0 M CH_3OH solution for 3000 s at 0.65 V potential.

peak potential of CO_{ads} oxidation on Pt−Cu BANDs negatively shift ca. 60 and 26 mV compared to those on commercial Pt black, indicating the adsorbed CO species on Pt−Cu BANDs surface are weaker than that on commercial Pt black. This result indicates that the incorporation of Cu with Pt plays an important role for improving the CO tolerance of elelctrocatalysts. Since the binding energy of Pt 4f in Pt−Cu BANDs is 0.41 eV lower than that in Pt black, the dramatic drop in the affinity of CO on Pt−Cu BANDs can be ascribed to the change of electron structure of Pt atom in Pt−Cu BANDs, based on d-band center theory.[58−60] Moreover, the existence of Cu also likely facilitates the effective CO removal because of geometric effect and bifunctional mechanism (i.e., the Cu metal disrupts

7305

dx.doi.org/10.1021/am500656j | ACS Appl. Mater. Interfaces 2014, 6, 7301−7308

the continuity of the Pt lattice and provides sites for OH adsorption).

The electrocatalytic activity and stability of Pt−Cu BANDs and Pt black for the MOR were further investigated by chronoamperometry at 0.65 V potential. During the whole reaction process, methanol oxidation current on Pt−Cu BANDs is higher than that on commercial Pt black (Figure 7B), confirming that the electrocatalytic activity of Pt−Cu BANDs is much better than that of Pt black. Considering their ultrafine grain size, alloy property, and dendritic structural feature, the enhanced electrocatalytic activity of Pt−Cu BANDs might be ascribed to their sufficient active sites, synergistic effects between Pt and Cu atoms, and high density of actively low-coordinated defective atoms on nanodendrites surface such as edge, corner, and surface stepped atoms.[1] At 3000 s, methanol oxidation currents on Pt−Cu BANDs and Pt black decrease to 14.7% and 4.8% of their initial value (taken at 20 s to avoid the contribution of the double-layer discharge and hydrogen adsorption),[61,62] respectively, indicating that the electrocatalytic stability of Pt−Cu BANDs is better than that of commercial Pt black. Long-term stability of catalysts were also investigated by continuous CV measurements. After 1000 cycles, the peak currents of methanol oxidation on Pt−Cu BANDs and Pt black decrease to 65% and 42% of their initial values, respectively (SI Figure S6), thus also indicating that Pt−Cu BANDs is more stable as an electrocatalyst for methanol oxidation. In general, the degradation of electrocatalytic performance originates from CO poisoning and nanoparticles migration/agglomeration during the anode reaction. Obviously, the high CO tolerance of Pt−Cu BANDs is responsible for improved stability of Pt−Cu BANDs for the MOR. In addition, no obvious morphological change occurs for Pt−Cu BANDs after chronoamperometry run, as revealed by TEM images (SI Figure S7). Mainly, the interconnected dendritic structure of Pt−Cu BANDs can effectively suppresses Ostwald ripening or grain growth of Pt−Cu BANDs, and consequently avoids the aggregation of Pt−Cu BANDs.[20,63−65] Thus, the interconnected dendritic structure of Pt−Cu BANDs is also responsible for their improved durability for the MOR. Meanwhile, the Pt/Cu atom ratio (56:44) in Pt−Cu BANDs after the chronoamperometry run is close to that (52:48) of the initial Pt−Cu BANDs (SI Figure S8). Previous reports demonstrated that Pt−Ag alloy nanostructures possessed excellent stability in acidic solution because alloying with Pt can greatly enhance the electrochemical stability of Ag.[66,67] Similarly, the high alloying degree of Pt−Cu BANDs may restrain leakage of Cu metal due to strong interaction between Pt and Cu atoms, which also contribute to high stability of Pt−Cu BANDs.

4. CONCLUSIONS

In summary, the Pt−Cu bimetallic nanodendrites with high alloying degree and high shape selectivity are synthesized by a facile wet-chemical coreduction method in a PAH-based aqueous system. Undoubtedly, the present aqueous based synthesis is more promising from an environmental standpoint, adding advantage over the use of toxic organic solvents. The formation of Pt−Cu alloy is attributed to the autocatalytic growth mechanism, which is supported by the fact that Cu^{2+} ion cannot be solely reduced under the same experimental conditions. The selective oxidative etching of Cu adatoms on preformed Pt seed surface plays a key role in formation of dendritic morphology of Pt−Cu alloy nanostructures, which is supported by facts that the irregular Pt−Cu multipods are

achieved under N_2-saturated conditions and the oxidative etching cannot occur on Pt nanocubes. In nature, the dendritic structures of Pt−Cu BANDs are favorable for reducing the Pt consumption, providing high surface area, and facilitating enhanced performance in electrocatalytic applications. Electrochemical measurements demonstrate that Pt−Cu BANDs exhibit superior MOR activity and long-term durability compared to commercial Pt black because of "synergistic effect" between Pt and Cu atoms (such as electronic effect, geometric effect, and bifunctional mechanism, etc.), unique interconnected nanostructures, and high CO tolerance. Thus, the superior electrocatalytic performance of Pt−Cu BANDs makes it a promising efficient anode elecctrocatalyst for the direct methanol fuel cells.

■ ASSOCIATED CONTENT

⑤ Supporting Information
Additional experimental details and additional characterization data. This material is available free of charge via the Internet at http://pubs.acs.org.

■ AUTHOR INFORMATION

Corresponding Authors
*Email: ndchenyu@gmail.com.
*Email: tangyawen@njnu.edu.cn.

Author Contributions
§M.G. and G.F. contributed equally to this work.

Notes
The authors declare no competing financial interest.

■ ACKNOWLEDGMENTS

■ REFERENCES

(1) Lim, B.; Lu, X.; Jiang, M.; Camargo, P. H. C.; Cho, E. C.; Lee, E. P.; Xia, Y. Facile Synthesis of Highly Faceted Multioctahedral Pt Nanocrystals through Controlled Overgrowth. *Nano Lett.* **2008**, *8*, 4043−4047.

(2) Wang, L.; Wang, H.; Nemoto, Y.; Yamauchi, Y. Rapid and Efficient Synthesis of Platinum Nanodendrites with High Surface Area by Chemical Reduction with Formic Acid. *Chem. Mater.* **2010**, *22*, 2835−2841.

(3) Wang, L.; Yamauchi, Y. Facile Synthesis of Three-Dimensional Dendritic Platinum Nanoelectrocatalyst. *Chem. Mater.* **2009**, *21*, 3562−3569.

(4) Wang, L.; Imura, M.; Yamauchi, Y. Tailored Design of Architecturally Controlled Pt Nanoparticles with Huge Surface Areas toward Superior Unsupported Pt Electrocatalysts. *Acs Appl. Mater. Inter.* **2012**, *4*, 2865−2869.

(5) Yeo, K. M.; Choi, S.; Anisur, R. M.; Kim, J.; Lee, I. S. Surfactant-Free Platinum-on-Gold Nanodendrites with Enhanced Catalytic Performance for Oxygen Reduction. *Angew. Chem., Int. Ed.* **2011**, *50*, 745−748.

(6) Yin, J.; Wang, J.; Li, M.; Jin, C.; Zhang, T. Iodine Ions Mediated Formation of Monomorphic Single-Crystalline Platinum Nanoflowers. *Chem. Mater.* **2012**, *24*, 2645−2654.

7306

dx.doi.org/10.1021/am500656j | *ACS Appl. Mater. Interfaces* 2014, 6, 7301−7308

(7) Wang, L.; Yamauchi, Y. Block Copolymer Mediated Synthesis of Dendritic Platinum Nanoparticles. *J. Am. Chem. Soc.* **2009**, *131*, 9152−9153.

(8) Mahmoud, M. A.; Tabor, C. E.; El-Sayed, M. A.; Ding, Y.; Wang, Z. L. A New Catalytically Active Colloidal Platinum Nanocatalyst: The Multiarmed Nanostar Single Crystal. *J. Am. Chem. Soc.* **2008**, *130*, 4590−4591.

(9) Wang, L.; Yamauchi, Y. Synthesis of Mesoporous Pt Nanoparticles with Uniform Particle Size from Aqueous Surfactant Solutions toward Highly Active Electrocatalysts. *Chem.—Eur. J.* **2011**, *17*, 8810−8815.

(10) Lim, B.; Xia, Y. Metal Nanocrystals with Highly Branched Morphologies. *Angew. Chem. Int.l Ed.* **2011**, *50*, 76−85.

(11) Watt, J.; Cheong, S.; Tilley, R. D. How to Control the Shape of Metal Nanostructures in Organic Solution Phase Synthesis for Plasmonics and Catalysis. *Nano Today* **2013**, *8*, 198−215.

(12) Liu, L.; Samjeske, G.; Nagamatsu, S.-i.; Sekizawa, O.; Nagasawa, K.; Takao, S.; Imaizumi, Y.; Yamamoto, T.; Uruga, T.; Iwasawa, Y. Enhanced Oxygen Reduction Reaction Activity and Characterization of Pt−Pd/C Bimetallic Fuel Cell Catalysts with Pt-Enriched Surfaces in Acid Media. *J. Phys. Chem. C* **2012**, *116*, 23453−23464.

(13) Ding, L. X.; Wang, A. L.; Li, G. R.; Liu, Z. Q.; Zhao, W. X.; Su, C. Y.; Tong, Y. X. Porous Pt−Ni−P Composite Nanotube Arrays: Highly Electroactive and Durable Catalysts for Methanol Electrooxidation. *J. Am. Chem. Soc.* **2012**, *134*, 5730−5733.

(14) Ding, L. X.; Li, G. R.; Wang, Z. L.; Liu, Z. Q.; Liu, H.; Tong, Y. X. Porous Ni@Pt Core−Shell Nanotube Array Electrocatalyst with High Activity and Stability for Methanol Oxidation. *Chem.—Eur. J.* **2012**, *18*, 8386−8391.

(15) Wang, W. Y.; Wang, D. S.; Liu, X. W.; Peng, Q.; Li, Y. D. Pt−Ni Nanodendrites with High Hydrogenation Activity. *Chem. Commun.* **2013**, *49*, 2903−2905.

(16) Lee, Y. W.; Kim, B. Y.; Lee, K. H.; Song, W. J.; Cao, G. Z.; Park, K. W. Synthesis of Monodispersed Pt−Ni Alloy Nanodendrites and Their Electrochemical Properties. *Inter. J. Electrochem. Sci.* **2013**, *8*, 2305−2312.

(17) Guo, S. J.; Dong, S. J.; Wang, E. K. Three-Dimensional Pt-on-Pd Bimetallic Nanodendrites Supported on Graphene Nanosheet: Facile Synthesis and Used as an Advanced Nanoelectrocatalyst for Methanol Oxidation. *ACS Nano* **2010**, *4*, 547−555.

(18) Wang, L.; Nemoto, Y.; Yamauchi, Y. Direct Synthesis of Spatially-Controlled Pt-on-Pd Bimetallic Nanodendrites with Superior Electrocatalytic Activity. *J. Am. Chem. Soc.* **2011**, *133*, 9674−9677.

(19) Lim, B.; Jiang, M. J.; Yu, T.; Camargo, P. H. C.; Xia, Y. N. Nucleation and Growth Mechanisms for Pd−Pt Bimetallic Nanodendrites and Their Electrocatalytic Properties. *Nano Res.* **2010**, *3*, 69−80.

(20) Fu, G.; Wu, K.; Lin, J.; Tang, Y.; Chen, Y.; Zhou, Y.; Lu, T. One-Pot Water-Based Synthesis of Pt−Pd Alloy Nanoflowers and Their Superior Electrocatalytic Activity for the Oxygen Reduction Reaction and Remarkable Methanol-Tolerant Ability in Acid Media. *J. Phys. Chem. C* **2013**, *117*, 9826−9834.

(21) Lim, B.; Jiang, M.; Camargo, P.; Cho, E.; Tao, J.; Lu, X.; Zhu, Y.; Xia, Y. Pd−Pt Bimetallic Nanodendrites with High Activity for Oxygen Reduction. *Science* **2009**, *324*, 1302−1305.

(22) Karthika, P.; Ataee-Esfahani, H.; Deng, Y. H.; Wu, K. C. W.; Rajalakshmi, N.; Dhathathreyan, K. S.; Arivuoli, D.; Ariga, K.; Yamauchi, Y. Hard-Templating Synthesis of Mesoporous Pt-Based Alloy Particles with Low Ni and Co Contents. *Chem. Lett.* **2013**, *42*, 447−449.

(23) Han, X. Y.; Wang, D. W.; Liu, D.; Huang, J. S.; You, T. Y. Synthesis and Electrocatalytic Activity of Au/Pt Bimetallic Nanodendrites for Ethanol Oxidation in Alkaline Medium. *J. Colloid Interface Sci.* **2012**, *367*, 342−347.

(24) Li, Y.; Wu, S.; Cui, X.; Wang, L.; Shi, X. Ultralow Platinum-Loading Bimetallic Nanoflowers: Fabrication and High-Performance Electrocatalytic Activity towards the Oxidation of Formic Acid. *Electrochem. Commun.* **2012**, *25*, 19−22.

(25) Zhang, J. T.; Ma, J. Z.; Wan, Y.; Jiang, J. W.; Zhao, X. S. Dendritic Pt−Cu Bimetallic Nanocrystals with a High Electrocatalytic Activity toward Methanol Oxidation. *Mater. Chem. Phys.* **2012**, *132*, 244−247.

(26) Porter, N. S.; Wu, H.; Quan, Z.; Fang, J. Shape-Control and Electrocatalytic Activity-Enhancement of Pt-Based Bimetallic Nanocrystals. *Acc. Chem. Res.* **2013**, *46*, 1867−1877.

(27) Deng, Y.-J.; Tian, N.; Zhou, Z.-Y.; Huang, R.; Liu, Z.-L.; Xiao, J.; Sun, S.-G. Alloy Tetrahexahedral Pd−Pt Catalysts: Enhancing Significantly the Catalytic Activity by Synergy Effect of High-Index Facets and Electronic Structure. *Chem. Sci.* **2012**, *3*, 1157−1161.

(28) Lee, K.; Kang, S. W.; Lee, S.-U.; Park, K.-H.; Lee, Y. W.; Han, S. W. One-Pot Synthesis of Monodisperse 5 nm Pd−Ni Nanoalloys for Electrocatalytic Ethanol Oxidation. *Acs Appl. Mater. Inter.* **2012**, *4*, 4208−4214.

(29) Hwang, B. J.; Tsai, Y. W.; Sarma, L. S.; Tseng, Y. L.; Liu, D. G.; Lee, J. F. Genesis of Bimetallic Pt−Cu Clusters in Reverse Micelles Investigated by In Situ X-ray Absorption Spectroscopy. *J. Phys. Chem. B* **2004**, *108*, 20427−20434.

(30) Niu, Z.; Wang, D.; Yu, R.; Peng, Q.; Li, Y. Highly Branched Pt−Ni Nanocrystals Enclosed by Stepped Surface for Methanol Oxidation. *Chem. Sci.* **2012**, *3*, 1925−1929.

(31) Vasquez, Y.; Sra, A. K.; Schaak, R. E. One-Pot Synthesis of Hollow Superparamagnetic CoPt Nanospheres. *J. Am. Chem. Soc.* **2005**, *127*, 12504−12505.

(32) Liu, Q.; Yan, Z.; Henderson, N. L.; Bauer, J. C.; Goodman, D. W.; Batteas, J. D.; Schaak, R. E. Synthesis of CuPt Nanorod Catalysts with Tunable Lengths. *J. Am. Chem. Soc.* **2009**, *131*, 5720−5721.

(33) Qiu, X.; Fu, G.; Zhao, Y.; Tang, Y.; Chen, Y.; Lu, T. Water-Based Synthesis and Sensing Application of Polyallylamine Functionalized Platinum Nanodendrite Assemblies. *J. Mater. Chem. A* **2013**, *1*, 14874−14878.

(34) Wang, C.; Chi, M.; Li, D.; Strmcnik, D.; van der Vliet, D.; Wang, G.; Komanicky, V.; Chang, K. C.; Paulikas, A. P.; Tripkovic, D.; Pearson, J.; More, K. L.; Markovic, N. M.; Stamenkovic, V. R. Design and Synthesis of Bimetallic Electrocatalyst with Multilayered Pt−Skin Surfaces. *J. Am. Chem. Soc.* **2011**, *133*, 14396−403.

(35) Shao, M.; He, G.; Peles, A.; Odell, J. H.; Zeng, J.; Su, D.; Tao, J.; Yu, T.; Zhu, Y.; Xia, Y. Manipulating the Oxygen Reduction Activity of Platinum Shells with Shape-Controlled Palladium Nanocrystal Cores. *Chem. Commun.* **2013**, *49*, 9030−2.

(36) Taylor, E.; Chen, S.; Tao, J.; Wu, L.; Zhu, Y.; Chen, J. Synthesis of Pt−Cu Nanodendrites through Controlled Reduction Kinetics for Enhanced Methanol Electro-oxidation. *ChemSusChem* **2013**, *6*, 1863−1867.

(37) Nosheen, F.; Zhang, Z. C.; Zhuang, J.; Wang, X. One-pot Fabrication of Single-Crystalline Octahedral Pt−Cu Nanoframes and Their Enhanced Electrocatalytic Activity. *Nanoscale* **2013**, *5*, 3660−3663.

(38) Mintsouli, I.; Georgieva, J.; Armyanov, S.; Valova, E.; Avdeev, G.; Hubin, A.; Steenhaut, O.; Dille, J.; Tsiplakides, D.; Balomenou, S.; Sotiropoulos, S. Pt−Cu Electrocatalysts for Methanol Oxidation Prepared by Partial Galvanic Replacement of Cu/Carbon Powder Precursors. *Appl. Catal., B* **2013**, *136*, 160−167.

(39) Liu, X. W.; Wang, W. Y.; Li, H.; Li, L. S.; Zhou, G. B.; Yu, R.; Wang, D. S.; Li, Y. D. One-Pot Protocol for Bimetallic Pt/Cu Hexapod Concave Nanocrystals with Enhanced Electrocatalytic Activity. *Sci. Rep.* **2013**, *3*, 01404.

(40) Zhang, J.; Yang, H. Z.; Martens, B.; Luo, Z. P.; Xu, D.; Wang, Y. X.; Zou, S. Z.; Fang, J. Y. Pt−Cu Nanoctahedra: Synthesis and Comparative Study with Nanocubes on their Electrochemical Catalytic Performance. *Chem. Sci.* **2012**, *3*, 3302−3306.

(41) Yin, A. X.; Min, X. Q.; Zhu, W.; Liu, W. C.; Zhang, Y. W.; Yan, C. H. Pt−Cu and Pt−Pd−Cu Concave Nanocubes with High-Index Facets and Superior Electrocatalytic Activity. *Chem.—Eur. J.* **2012**, *18*, 777−782.

(42) Yu, X. F.; Wang, D. S.; Peng, Q.; Li, Y. D. High Performance Electrocatalyst: Pt−Cu Hollow Nanocrystals. *Chem. Commun.* **2011**, *47*, 8094−8096.

(43) Jiang, Y.; Jia, Y.; Zhang, J.; Zhang, L.; Huang, H.; Xie, Z.; Zheng, L. Underpotential Deposition-Induced Synthesis of Composition-Tunable Pt Cu Nanocrystals and Their Catalytic Properties. *Chem.—Eur. J.* **2013**, *19*, 3119−3124.

(44) Yu, X. F.; Wang, D. S.; Peng, Q.; Li, Y. D. Pt−M (M = Cu, Co, Ni, Fe) Nanocrystals: From Small Nanoparticles to Wormlike Nanowires by Oriented Attachment. *Chem.—Eur. J.* **2013**, *19*, 233−239.

(45) Gupta, G.; Slanac, D. A.; Kumar, P.; Wiggins-Camacho, J. D.; Wang, X. Q.; Swinnea, S.; More, K. L.; Dai, S.; Stevenson, K. J.; Johnston, K. P. Highly Stable and Active Pt−Cu Oxygen Reduction Electrocatalysts Based on Mesoporous Graphitic Carbon Supports. *Chem. Mater.* **2009**, *21*, 4515−4526.

(46) Liu, Z. C.; Koh, S.; Yu, C. F.; Strasser, P. Synthesis, Dealloying, and ORR Electrocatalysis of PDDA-Stabilized Cu-Rich Pt Alloy Nanoparticles. *J. Electrochem. Soc.* **2007**, *154*, B1192−B1199.

(47) Xia, B. Y.; Wu, H. B.; Wang, X.; Lou, X. W. One-Pot Synthesis of Cubic PtCu₃ Nanocages with Enhanced Electrocatalytic Activity for the Methanol Oxidation Reaction. *J. Am. Chem. Soc.* **2012**, *134*, 13934−13937.

(48) Xu, D.; Liu, Z.; Yang, H.; Liu, Q.; Zhang, J.; Fang, J.; Zou, S.; Sun, K. Solution-Based Evolution and Enhanced Methanol Oxidation Activity of Monodisperse Platinum−Copper Nanocubes. *Angew. Chem. Inter. Ed.* **2009**, *48*, 4217−4221.

(49) Mazumder, V.; Sun, S. Oleylamine-mediated Synthesis of Pd Nanoparticles for Catalytic Formic Acid Oxidation. *J. Am. Chem. Soc.* **2009**, *131*, 4588−4589.

(50) Fu, G.; Zhao, R.; Ding, L.; Tao, L.; Lin, J.; Chen, Y.; Tang, Y.; Zhou, Y.; Lu, T. Synthesis, Self-Assembly, and Electrocatalysis of Polyallylamine-Functionalized Platinum Nanocubes. *ChemPlusChem.* **2013**, *78*, 623−627.

(51) Fu, G.; Wu, K.; Jiang, X.; Tao, L.; Chen, Y.; Lin, J.; Zhou, Y.; Wei, S.; Tang, Y.; Lu, T.; Xia, X. Polyallylamine-directed Ggreen Synthesis of Platinum Nanocubes. Shape and Electronic Effect Codependent Enhanced Electrocatalytic Activity. *Phys. Chem. Chem. Phys.* **2013**, *15*, 3793−3802.

(52) Fu, G.; Jiang, X.; Tao, L.; Chen, Y.; Lin, J.; Zhou, Y.; Tang, Y.; Lu, T. Polyallylamine Functionalized Palladium Icosahedra: One-Pot Water-Based Synthesis and Their Superior Electrocatalytic Activity and Ethanol Tolerant Ability in Alkaline Media. *Langmuir* **2013**, *29*, 4413−4420.

(53) Fu, G.; Jiang, X.; Ding, L.; Tao, L.; Chen, Y.; Tang, Y.; Zhou, Y.; Wei, S.; Lin, J.; Lu, T. Green Synthesis and Catalytic Properties of Polyallylamine Functionalized Tetrahedral Palladium Nanocrystals. *Appl. Catal., B* **2013**, *138−139*, 167−174.

(54) Chu, Y.-T.; Chanda, K.; Lin, P.-H.; Huang, M. H. Aqueous Phase Synthesis of Palladium Tripod Nanostructures for Sonogashira Coupling Reactions. *Langmuir* **2012**, *28*, 11258−11264.

(55) Chen, Y.-H.; Hung, H.-H.; Huang, M. H. Seed-Mediated Synthesis of Palladium Nanorods and Branched Nanocrystals and Their Use as Recyclable Suzuki Coupling Reaction Catalysts. *J. Am. Chem. Soc.* **2009**, *131*, 9114−9121.

(56) Zhang, L.; Zhang, J.; Kuang, Q.; Xie, S.; Jiang, Z.; Xie, Z.; Zheng, L. Cu²⁺-Assisted Synthesis of Hexoctahedral Au−Pd Alloy Nanocrystals with High-Index Facets. *J. Am. Chem. Soc.* **2011**, *133*, 17114−17117.

(57) Hoover, N. N.; Auten, B. J.; Chandler, B. D. Tuning Supported Catalyst Reactivity with Dendrimer-templated Pt−Cu Nanoparticles. *J. Phys. Chem. B* **2006**, *110*, 8606−8612.

(58) Hammer, B.; Nørskov, J. Electronic Factors Determining the Reactivity of Metal Surfaces. *Surf. Sci.* **1995**, *343*, 211−220.

(59) Mavrikakis, M.; Hammer, B.; Nørskov, J. K. Effect of Strain on the Reactivity of Metal Surfaces. *Phys. Rev. lett.* **1998**, *81*, 2819−2822.

(60) Hammer, B.; Morikawa, Y.; Nørskov, J. K. CO Chemisorption at Metal Surfaces and Overlayers. *Phys. Rev. lett.* **1996**, *76*, 2141−2144.

(61) Jiang, J.; Kucernak, A. Electrocatalytic Properties of Nanoporous PtRu Alloy towards the Electrooxidation of Formic Acid. *J. Electroanal. Chem.* **2009**, *630*, 10−18.

(62) Yu, X.; Pickup, P. Novel Pd−Pb/C Bimetallic Catalysts for Direct Formic Acid Fuel Cells. *J. Power Sources* **2009**, *192*, 279−284.

(63) Zhang, G.; Zhang, L.; Shen, L.; Chen, Y.; Zhou, Y.; Tang, Y.; Lu, T. Synthesis and Electrocatalytic Properties of Palladium Network Nanostructures. *ChemPlusChem.* **2012**, *77*, 936−940.

(64) Jia, F.; Wang, F.; Lin, Y.; Zhang, L. Microwave-Induced Formation of Platinum Nanostructured Networks with Superior Electrochemical Activity and Stability. *Chem.—Eur. J.* **2011**, *17*, 14603−14610.

(65) Xu, J.; Fu, G.; Tang, Y.; Zhou, Y.; Chen, Y.; Lu, T. One-Pot Synthesis of Three-Dimensional Platinum Nanochains Networks as Stable and Active Electrocatalyst for Oxygen Reduction Reaction. *J. Mater. Chem.* **2012**, *22*, 13585−13590.

(66) He, W.; Wu, X.; Liu, J.; Zhang, K.; Chu, W.; Feng, L.; Hu, X.; Zhou, W.; Xie, S. Pt-Guided Formation of Pt−Ag Alloy Nanoislands on Au Nanorods and Improved Methanol Electro-oxidation. *J. Phys. Chem. C* **2009**, *113*, 10505−10510.

(67) Kim, K.; Kim, K. L.; Shin, K. S. Coreduced Pt/Ag Alloy Nanoparticles: Surface-Enhanced Raman Scattering and Electrocatalytic Activity. *J. Phys. Chem. C* **2011**, *115*, 23374−23380.